A Theoretical Study of the $P^+ + SH_2$ Reaction: Potential Energy Surfaces and Reaction Dynamics

Jesús R. Flores* and Carlos M. Estévez

Departamento de Química Física y Química Orgánica, Facultad de Ciencias, Campus de Vigo, Universidad de Vigo, 36200 Vigo, Spain

Received: May 31, 2000; In Final Form: August 29, 2000

A theoretical study of the reaction of P^+ with SH_2 has been carried out. We employed an approximate classical trajectory method to deal with the capture process and a RRKM-type approach to analyze the evolution of the $(PSH_2)^+$ complex. The trajectory computations allowed for nonadiabatic transitions whose probabilities were computed through the Landau−Zener and Rosen−Zener−Demkov models. The potential energy surfaces were computed with the G2(QCI) method for the local minima and with the MR-AQCC and PMP2 methods for the energy profiles. This reaction is interesting from the theoretical point of view, for it generates electron-transfer products as well as two other products. The corresponding reaction paths are identified, and estimates of the reaction rates are given. The experimental values of the PSH^+/PS^+ branching ratio could not be explained without considering the major role of the singlet potential energy surface. The results even point to a $HPSH^+$-$(^1A')$ species, which is the global minimum of the potential surface, as the reaction intermediate from which both products are generated.

I. Introduction

Gas-phase ion−molecule reactions play a crucial role in the chemistry of the terrestrial atmosphere and the low-density clouds filling the space between the stars, the interstellar clouds,[1] and the reactions have been the subject of intense experimental[2] and theoretical work.[2,3] The reaction of P^+ with SH_2 has been studied experimentally by Adams and co-workers in the gas phase through a selected ion flow tube (SIFT) apparatus at $T = 300$ K.[4] This is an especially interesting case because there are three channels:

$$P^+ + SH_2 \rightarrow P + SH_2^+ \qquad (31\%)$$

$$P^+ + SH_2 \rightarrow PS^+ + H_2 \qquad (12\%)$$

$$P^+ + SH_2 \rightarrow PSH^+ + H \qquad (57\%)$$

The numbers in parentheses indicate the amount of corresponding product. The fact that we have an electron-transfer channel and two other reaction channels implies that this reaction is an ideal case for testing some of the theoretical methods usually employed for the ion−molecule reactions. The channels giving PS^+ and PSH^+ have been suggested as important steps in the production of molecules containing P−S bonds in interstellar chemistry.[5] Finally, since a number of similar reactions between atomic ions and small hydrides are believed to be of primary importance in interstellar chemistry, the present case can be viewed to some extent as a model for the reactions.

When trying to establish general patterns in the dynamics of ion−molecule reactions, we must sort out several uncertainties. For instance, the electron-transfer process might take place through a long-range interaction but could also be a result of the evolution of the system on several potential energy surfaces (PES) at short range. Besides, it has been suggested that when there are several nearly degenerate potential surfaces for the interaction of reactants, the observed rate coefficient should be almost coincident with the capture rate scaled by the fraction of the potential surfaces that are attractive.[6,7] However, a thorough test of this hypothesis would require systematically computing the ground and low-lying electronic states and the capture rates for a large number of reactions. Even though complementing experimental studies of ion−molecule reactions with simple computations of capture rates is quite a common practice, adequately computed energy profiles of the electronic states are much more scarce, for ab initio studies normally focus on the characterization of the lowest-lying reaction intermediates.

The present reaction is particularly interesting because (i) the phosphorus cation has three nearly degenerate levels corresponding to the ^3P term and (ii) the enthalpy of the electron-transfer reaction $P^+ + SH_2 \leftrightarrow P + SH_2^+(^2B_1)$ computed as the difference between the ionization energies of hydrogen sulfide and phosphorus[8] is just -1.7 ± 1.2 kJ/mol. This implies that the nonadiabatic transition into electron-transfer products might occur in the capture step. In addition, it has been suggested that the generation of both $PO^+ + H_2$ and $POH^+ + H$ in the reaction of P^+ with water might proceed through a singlet $HPOH^+(^1A')$ intermediate.[9] In this case, the branching ratio could be explained successfully by applying statistical theory, combined with using potential surfaces of G2 quality.[10] A quick look at the published potential energy surfaces for the reaction of second-row cations and small molecules indicates that intersystem crossing processes could be quite common indeed, so the longest-living reaction intermediate could often be a species of the lowest spin multiplicity.

The purpose of the present paper is to gain insight into the dynamics of this ion−molecule reaction, which may also represent the dynamics of many reactions of atomic ions with small molecules. The several reaction channels for which branching ratios are known from experiment might be invaluable.

10.1021/jp001968k CCC: $19.00
Published on Web 11/04/2000

II. Theoretical Approach

We will distinguish two steps in the dynamics of the $P^+ + SH_2$ reaction: (i) the capture step and (ii) the evolution of the $(PSH_2)^+$ complex, which leads ultimately to the products PS^+ and PSH^+.

The present study involves several parts:

(a) First, we computed the reaction coordinates and energy profiles for all relevant electronic states using ab initio methods.

(b) A complete high-level ab initio study of the potential surfaces of the $(PH_2S)^+$ systems was made for the lowest-lying triplet and singlet states, including the reactants and products.

(c) We studied the dynamics of the capture step through a classical trajectory method. This study has involved all relevant electronic states of the reactants (arising from the ^3P term of P^+) and has allowed for all possible nonadiabatic transitions. Trajectories may be classified as (i) nonreactive if they produce the reactants on any of the electronic states arising from the ^3P term of P^+, (ii) electron-transfer if they lead to $P + SH_2^+(^2B_1)$, or (iii) reactiveif they initially derive a $PSH_2^+(^3A'')$ complex that may ultimately evolve to generate PS^+, PSH^+, and also $P + SH_2^+$, which is an additional electron-transfer channel. The method permits us to determine the populations of total energies and angular momentum for any channel, which are expressed through the distribution function $f(E,J)$.

(d)The evolution of the $(PH_2S)^+$ complex was studied through RRKM theory not in the standard way, which employs a thermal distribution, but by using the distribution corresponding to the trajectories that produce the complex.

III. Computational Details of the ab Initio Computations

The computation of minima has been carried out normally at the MP2=full/6-31G(d) level, although in some particular cases the QCISD/6-31G(d) method was employed too.[10] The saddle points have been located at both the MP2=full/6-31G(d) and QCISD/6-31G(d) levels; their existence has often been confirmed at the QCISD/6-311++G(d,p) level. Vibrational frequencies have been determined analytically at the MP2=full/6-31G(d) level for both local minima and saddle points. The relative energies (with respect to the reactants) of the local minima have been computed at the so-called G2(QCI) level.[11] This G2(QCI) method is directly related to the G2 method.[12] It employs QCISD(T)/6-311+G(3df,2p)//MP2=full/6-31G(d) electronic energies, scaled HF/6-31G(d) zero-point vibrational energies (ZPVE), and a high-level correction aimed at complementing the part of the correlation energy not captured by the QCISD(T) computation. Our only modification is the use of unscaled MP2=full/6-31G(d) ZPVE frequencies; this was considered more reliable for saddle points in a small molecular system.

The relative energies of the saddle points were obtained by adding QCISD(T)/6-311+G(3df,2p)//QCISD/6-31G(d) electronic energy differences and unscaled MP2=full/6-31G(d) ZPVE differences, both computed with respect to a particular minimum, to the relative energy of the latter. The reference minimum was selected according to its proximity to the saddle point on the potential energy surface. We decided that the QCISD/6-31G(d) optimized geometries would be more reliable than the MP2=full/6-31G(d) ones, as the superiority of the QCI method over MP2 for this purpose has already been established.[13]

The reaction coordinates for the capture process have been obtained at the QCISD/6-31G(d,p) level in the following way:

(a) A C_{2v} coordinate was determined for the $^3A_2$ state (which correlates at large P−S distances with the reactants, P^+ and SH_2). A number of geometry optimizations have been performed for several P−S distances by keeping this variable constant and optimizing the other variables with the additional constraint of maintaining the C_{2v} symmetry.

(b) A C_s coordinate was determined for the ground state; this is always an $^3A''$ state and correlates with $P + SH_2^+$ for large P−S distances. This time, the additional constraint is the C_s symmetry, meaning the geometries with two equivalent S−H bonds.

At each point of the coordinates, several computations were carried out at correlated levels, all using a complete active space (CAS) type of MCSCF reference wave function.[14] The (correlation-consistent) cc-pVTZ has been employed in all cases.[15] The use of the MCSCF reference wave functions is indispensable because, leaving aside the spin−orbit and other interactions, we have four nearly degenerate electronic states—namely, $^3B_2(0)$, which correlates with the electron-transfer products at large P−S distances, and $^3A_2$, $^3B_2(1)$, and $^3B_1$, which correlate with the reactants. Note that all states would be A'' in C_s symmetry (two equivalent S−H bonds) with the exception of B_1, which would be A'.

The active space of the CASSCF wave functions may be specified as C_{2v} [$9a_1$, $3b_1$, $4b_1$, $4b_2$] and C_s [12a', 13a', 14a', 4a''']. In both cases, the wave functions contain four active electrons.

We have computed a C_{2v} energy profile for the $^3A_2$ state and a C_s energy profile for the lowest-lying $^3A''$ state using the corresponding reaction coordinates. In both cases, the reference (CASSCF) wave functions were optimized for the corresponding state, enforcing only the C_s symmetry. Using these reference wave functions, we made averaged quadratic coupled-cluster (AQCC) computations; the AQCC wave function included all single and double spin−orbital substitutions in the reference wave function, leaving aside the core orbitals. The AQCC method[16] can be considered a variant of the ACPF method,[17] which can be viewed as a size-consistent MRCISD method.

To obtain energy differences, we used configuration interaction wave functions generated from all possible single and double spin−orbital substitutions in the reference wave functions, excluding the core orbitals. In this case, the reference wave function was optimized with C_s symmetry for a mixture of the three $^3A''$ states which were given equal weight.

Using the C_{2v} and C_s energy profiles computed at the AQCC level and the MRCISD energy differences, we have built energy profiles for all states for both C_{2v} and C_s symmetries. These energy profiles were used later to obtain the PES for the four electronic states through a procedure to be described later.

The MCSCF- and MRCI-type computations have been made with the COLUMBUS program system;[18] the rest of the ab initio computations have been carried out with the GAUSSIAN94 program package.[19]

IV. Potential Energy Surface of the $(PSH_2)^+$ System

IV.1. Local Minima and Saddle Points. The local minima and saddle points of the lowest triplet and singlet surfaces are depicted in Figures 1 and 2, which include the MP2=full/6-31G(d) geometrical parameters. (The qcisd/6-31G(d) geometries and other details are available from the authors upon request.) The relative energies are presented in Table 1. Scheme 1 arranges the reactants, products, minima, and saddle points according to their energies and connects them with lines representing the processes (to keep the diagram simple, we did not delineate some processes not having saddle points). There is a previous study of the triplet potential surface of the $(PSH_2)^+$

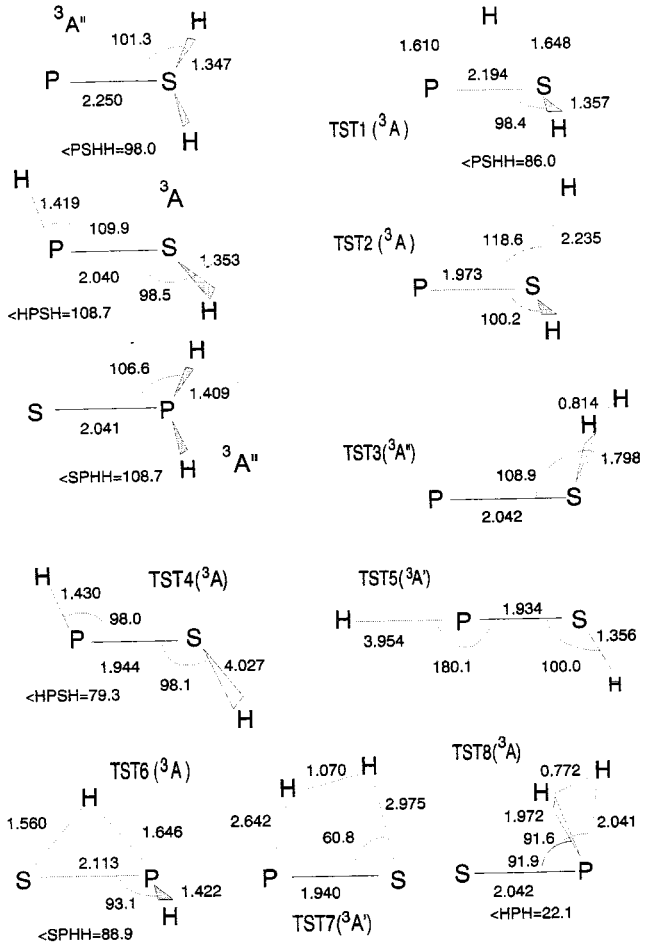

Figure 1. MP2=full/6-31G(d) optimized gometries (Å and deg) and electronic states of the local minima and saddle points (TSTn) of the triplet potential energy surface.

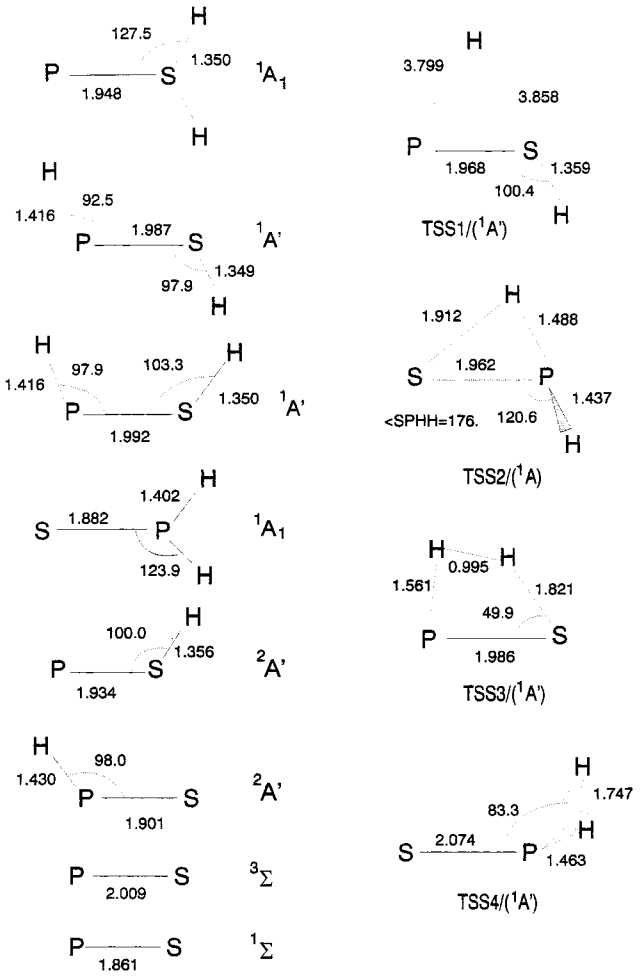

Figure 2. MP2=full/6-31G(d) optimized geometries (Å and degr) and electronic states of the local minima and saddle points (TSSn) of the singlet potential energy surface and some of the products. (SH_2: d(S−H) = 1.339, ∠HSH = 93.4. SH_2^+(2B1): d(S−H) = 1.351, ∠HSH = 94.7. H_2: d(H−H) = 0.736. Saddle-point $HPS^+(^2A')$ ↔ $PSH^+(^2A')$: d(P−S) = 1.803, d(S−H) = 2.078, ∠PSH = 116.4.)

system carried out at the MP4/6-311G(d,p)//HF/6-31G(d,p) level,[21] which was state-of-the-art at the time it was presented but cannot compete in accuracy with the G2(QCI) method in the present work; this quality difference is responsible for the significant discrepancies in the relative energies of several species, so we will not make any further comments on them.

We found three local minima on the triplet surface, PSH_2^+-($^3A''$), $SPH_2^+(^3A'')$, and $HPSH^+(^3A)$, ordered in increasing energy. However, they are rather close in energy and quite deep with respect to the reactants, even though the first species has a rather loose P−S bond.

$PSH_2^+(^3A'')$ may undergo isomerization into $HPSH^+(^3A)$

SCHEME 1: Representation of the Lowest-Lying Singlet and Triplet Potential Surfaces

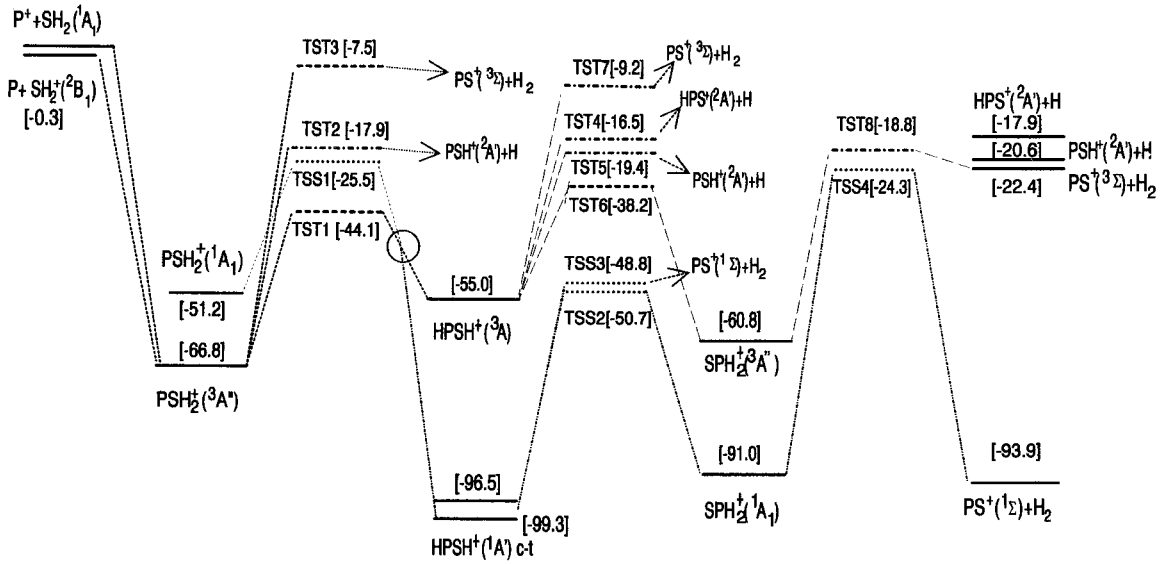

TABLE 1: MP2=full/6-31G(d) Zero-Point Vibrational Energies and Energy Differences (Including Electronic and Vibrational Contributions)[a]

	ZPVE (Hartree)	ΔE (kcal/mol)
$P^+ + SH_2$	0.01573	0.0
$P + SH_2^+(^2B_1)$	0.01538	−0.3
$PS^+(^1\Sigma) + H_2$	0.01212	−93.9
$PS^+(^3\Sigma) + H_2$	0.01151	−22.4
$PSH^+(^2A') + H$	0.00988	−20.6
$HPS^+(^2A') + H$	0.00873	−17.9
$PSH_2^+(^3A'')$	0.01942	−66.8
$HPSH^+(^3A)$	0.02195	−55.0
$SPH_2^+(^3A'')$	0.01779	−60.8
TST1/P(H)SH$^+$(^{3}A)[b]	0.01115	−44.1
TST2/PSH−H$^+$(^{3}A)[b]	0.01114	−17.9
TST3/PS$^+$−H$_2$(^{3}A″)[b]	0.01449	−7.5
TST4/HPS$^+$−H(^{3}A)[c]	0.00892	−16.5
TST5/H−PSH$^+$(^{3}A′)[c]	0.01024	−19.4
TST6/HP(H)S$^+$(^{3}A)[c]	0.01431	−38.2
TST7/P(H$_2$)S$^+$(^{3}A′)[c]	0.00974	−9.2
TST8/H$_2$−SP$^+$(^{3}A)[d]	0.01342	−18.8
$PSH_2^+(^1A_1)$	0.01879	−51.2
$HPSH^+(^1A')$t	0.01959	−99.3
$HPSH^+(^1A')$[d]	0.01919	−96.5
$SPH_2^+(^1A_1)$	0.01934	−91.0
TSS1/P(H)SH$^+$(^{1}A′)[e]	0.01002	−25.5
TSS2/HP(H)S$^+$(^{1}A)[f]	0.01385	−50.7
TSS3/P(H$_2$)S$^+$(^{1}A″)[g]	0.01457	−48.8
TSS4/H$_2$−PS$^+$(^{1}A′)[h]	0.01545	−24.3

[a] For the local minima, the G2(QCI) approach was used. The relative energies of the transition states were computed using a QCISD/6-311+G(3df,2p) electronic energy difference with respect to a reference minimum, identified in the footnote. [b] $PSH_2^+(^3A'')$. [c] $HPSH^+(^3A)$. [d] $SPH_2^+(^3A'')$. [e] $PSH^+(^2A') + H$. [f] $HPSH^+(^1A')$t. [g] $PS^+(^1\Sigma) + H_2$. [h] $SPH_2^+(^1A_1)$. $E_0(P^+ + SH_2) = -739.365\,942$ Hartrees. E_0 includes electronic, vibrational, and high-level corrections (see ref 11 and section III).

through the transition state TST1(^{3}A), which can also be seen as the saddle point for the straight insertion of the phosphorus cation into the S−H bond of hydrogen sulfide. But it may also generate $PSH^+(^2A')$ through TST2(^{3}A) and $PS^+(^3\Sigma) + H_2$ through TST3(^{3}A″).

$HPSH^+(^3A)$ may generate both $PSH^+(^2A')$ and $HPS^+(^2A')$ through the transition states TST4(^{3}A) and TST5(^{3}A), respectively, and also $PS^+(^3\Sigma) + H_2$ through TST7(^{3}A′). It may isomerize as well into $SPH_2^+(^3A'')$ via TST6(^{3}A).

We could not locate a saddle point for the generation of $SPH^+(^2A')$ from $SPH_2^+(^3A")$, but the TST8(^{3}A) structure appears to be a neat saddle point.

We found four minima on the lowest singlet surface: $PSH_2^+(^1A_1)$, $SPH_2^+(^1A_1)$, *cis*-$HPSH^+(^1A')$, and *trans*-$HPSH^+(^1A')$; the last species is precisely the absolute minimum of the potential surface. Both singlet SPH_2^+ and $HPSH^+$ lie below their triplet counterparts, whereas $PSH_2^+(^1A_1)$ is clearly higher in energy. The isomerization of $PSH_2^+(^3A'')$ may entail intersystem crossing; the degree of efficiency in such a process is critical to the dynamics of the system (see Scheme 1). $HPSH^+(^1A')$ may surmount the saddle point TSS3(^{1}A′) to produce $PS^+(^1\Sigma^+)$ or isomerize into $SPH_2^+(^1A_1)$ via TSS2(^{1}A′). $SPH_2^+(^1A_1)$ may generate $PS^+(^1\Sigma^+)$ through TSS4(^{1}A′).

Energy profiles were computed for the P−H and S−H bond-breaking processes of $HPSH^+(^1A')$ and $SPH_2^+(^1A_1)$.

We also paid some attention to the computation of the reaction energies, which was carried out at several levels in addition to G2(QCI) (namely, CBS-Q[22] and CBS-QB3).[23] The CBS reaction energies corresponding to the products PSH^+/HPS^+ and $PS^+(^3\Sigma)$ are about 3 kcal/mol deeper; this is mostly a consequence of the empirical correction for spin contamination in these methods. However, G2(QCI) seems to be more reliable than the CBS method for the electron-transfer reaction, where CBS-Q even gives the wrong sign.

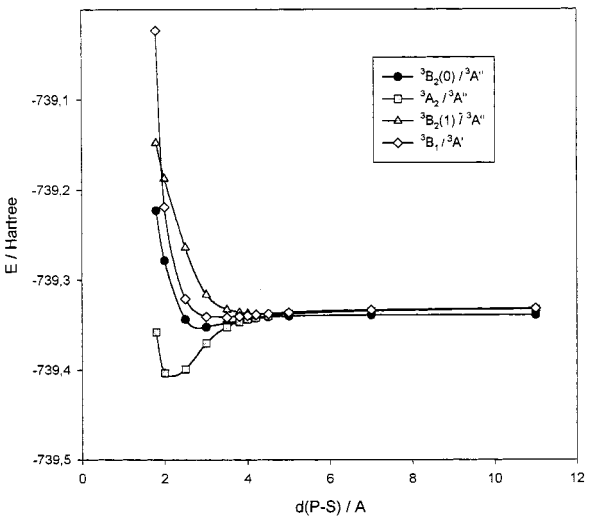

Figure 3. Energy profiles for C_{2v} geometries; electronic states are classified according to both the C_{2v} and C_s (two equivalent S−H bonds) symmetry species.

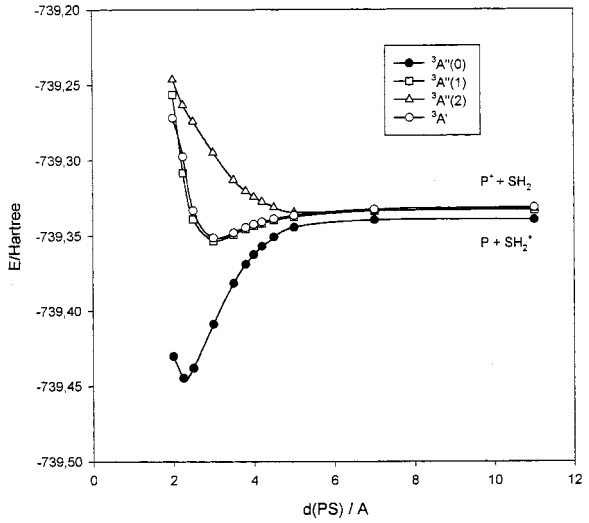

Figure 4. Energy profiles for C_s geometries (two equivalent S-H bonds).

IV.2. Energy Profiles and Modeling the PES for the Capture Step. As indicated above, we computed C_{2v} and C_s energy profiles for the capture step; they are depicted in Figures 3−6. The corresponding energies are given in Figures 3 and 4. Comparing the two sets of profiles and Tables 2−4, we immediately see that at distances close to the minimum $PSH_2^+(^3A'')$, the lowest state is much deeper in the C_s profile than in the C_{2v} profile.

The $^3A_2$ state crosses the $^3B_2(0)$ state at approximately d(P−S) = 4.15 D; since both states become $^3A''$ at C_s geometries, this point is the apex of a conical intersection. Note also that the $^3B_2$ states get closer until approximately d(P−S) = 4.4 D and then start to diverge; i.e., there is an avoided crossing. Both structures are crucial in the dynamics of the capture step. Only the lowest-lying state ($^3B_2(0)$ in the long-range region) has a deep minimum at the short range; the reaction process should entail a transition to this state and the formation of a highly energized $PSH_2^+(^3A'')$ species that would ultimately yield both PS^+ and $(PSH)^+$. Furthermore, breaking the P−S bond of $PSH_2^+(^3A'')$ would give mostly the electron-transfer products.

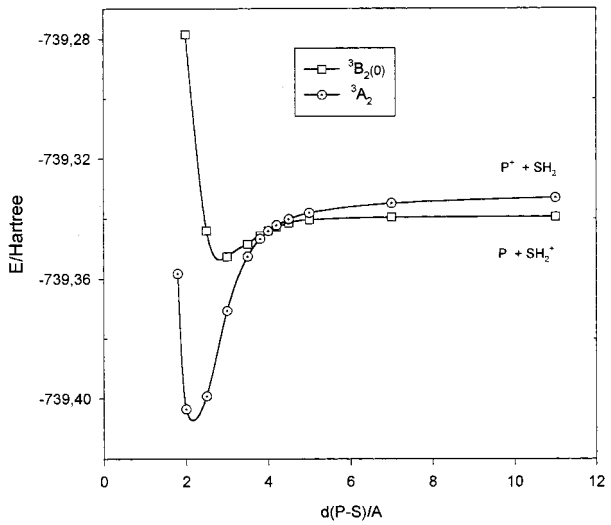

Figure 5. C_{2v} projection of the $^3A_2-^3B_2(0)$ conical intersection.

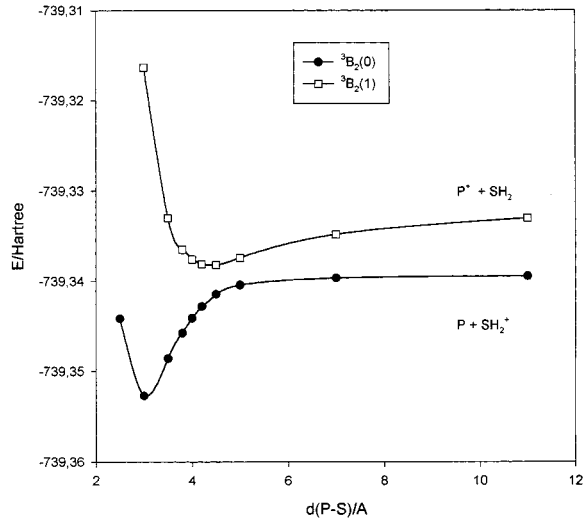

Figure 6. C_{2v} projection of the avoided crossing of the $^3B_2$ states.

TABLE 2: Zero-Point Reaction Energies (in kcal/mol) Computed at Several Levels[a]

	P + $SH_2^+(^2B_1)$	$PS^+(^1\Sigma)$ + H_2	$PS^+(^3\Sigma)$ + H_2	$PSH^+(^2A')$ + H	$HPS^+(^2A')$ + H
G2(QCI)	−0.3	−93.9	−22.4	−20.6	−17.9
CBS-Q	0.2	−93.4	−25.1	−23.0	−21.3
CBS-QB3	−0.1	−93.1	−25.3	−23.2	−21.1

[a] $E_0(P^+ + SH_2) = -739.365\,942$ Hartrees (G2(QCI)), −739.366 536 Hartrees (CBS-Q), and −739.368 16 Hartrees (CBS-QB3).

However, electron transfer may also happen via a transition to the lowest-lying state after a rebound on the highest-lying surfaces.

The PES of the capture step are modeled by combining diabatic potentials and coupling functions; both include parameters which are determined by fitting to the ab initio potentials. The diabatic potentials include both long and short-range parts. The long-range parts are given the well-known asymptotic expressions provided by Buckingham, for instance[24]

$$V_{lr}(r,\theta) = -(q\mu/r^2)\cos\theta + qQ(3\cos^2\theta - 1)/2r^3 - q^2\alpha/2r^4 - q^2(\alpha_{||} - \alpha_{\perp})(3\cos^2\theta - 1)/6r^4 \quad (1)$$

For the PES corresponding to the reactants, we employed a charge−dipole, charge−polarizability, charge−polarizability-anisotropy, or charge−quadrupole potential, while for the potential surface corresponding to the electron-transfer products, we employed a flat potential; this was found to be better than a charge−polarizability potential because the degree of polarization of P is heavily dependent on the orientation and not adequately reproduced by the former expression. (Experimental values: $\mu = 0.97$ D Å, $\alpha' = 3.78 \times 10^{-24}$ cm^3 [33]. Q taken as $\Theta_{zz} - 2z'$, $\mu = 0.0313$ D Å, $\alpha_{||}' - \alpha_{\perp}' = -0.42 \times 10^{-24}$ cm^3 [33], computed at the MP2=full/6-311++G(3df,2p) level. r is the P−S distance.) Given that the conical intersection and the avoided crossing appear at distances where short-term and repulsive interactions are not negligible, it was necessary to include short-range parts in the diabatic potentials. We employed an exponential expression of the radial coordinate. The $^3B_1$ and $^3B_2$ states were finally represented as follows:

$$^3B_1 \rightarrow V_d(r,\theta) = E^{\infty} + V_{lr}(r,\theta) + Ae^{-\alpha_0 r}$$

$$^3B_2(0,1) \rightarrow V_d(r,\theta) = E^{\infty} + V_{lr}(r,\theta) + A_1e^{-\alpha_1 r}(1 - e^{-r/f}) + A_2e^{-\alpha_2 r}e^{-r/f} \quad (2)$$

(The values, in Hartrees, Å^{-1}, or Å, are $A = 15.857$, $\alpha_0 = 2.0733$, $A_2 = 3.2723$, $A_1 = 20.0794$, $\alpha_2 = 1.2401$, $\alpha_1 = 2.6269$, and $f = 2$.)

The differences in the expressions of both B_2 states are the electronic energy at infinity and the long-range potential, which is just zero for $^3B_2(0)$; the repulsive part is common.

The $^3A_2$ state is special because it has an additional large component resulting from the formation of a chemical bond, which we will call $V_c(r)$. Note that for C_{2v} geometries, there is no interaction between this state and any other in the set; those interactions take place only at less symmetrical geometries and are important for the variation of the corresponding potential surface with the angle at short range. The expression given to

TABLE 3: C_{2v} Energy Profiles (in Hartrees) Computed at the MRCISD/cc-pVTZ Level

d(PS)/Å	$^3B_2(0)$	$^3A_2$	$^3B_2(1)$	$^3B_1$
30.0	−739.339 36	−739.332 20	−739.33220	−739.331 11
20.0	−739.339 37	−739.332 36	−739.332 36	−739.331 28
11.0	−739.339 43	−739.333 07	−739.333 02	−739.331 96
7.0	−739.339 63	−739.334 94	−739.334 79	−739.333 69
5.0	−739.340 40	−739.338 15	−739.337 36	−739.336 29
4.5	−739.341 42	−739.340 24	−739.338 15	−739.337 71
4.2	−739.342 79	−739.342 25	−739.338 06	−739.338 83
4.0	−739.344 09	−739.344 15	−739.337 54	−739.339 69
3.8	−739.345 71	−739.346 73	−739.336 46	−739.340 61
3.5	−739.348 55	−739.352 56	−739.332 95	−739.341 85
3.0	−739.352 68	−739.370 60	−739.316 34	−739.341 00
2.5	−739.344 12	−739.399 19	−739.263 76	−739.320 84
2.0	−739.278 55	−739.403 57	−739.187 12	−739.218 82
1.8	−739.222 94	−739.358 30	−739.147 38	−739.023 04

TABLE 4: C_s Energy Profiles (in Hartrees) Computed at the MRCISD/cc-pVTZ level

d(PS)/Å	$^3A''(0)$	$^3A''(1)$	$^3A''(2)$	$^3A'$
11.0	−739.339 36	−739.333 07	−739.332 28	−739.331 35
7.0	−739.339 58	−739.333 70	−739.333 50	−739.332 56
5.0	−739.344 17	−739.337 42	−739.334 47	−739.336 43
4.5	−739.350 67	−739.339 67	−739.331 05	−739.338 65
4.2	−739.356 85	−739.341 69	−739.327 45	−739.340 65
4.0	−739.362 26	−739.343 36	−739.324 13	−739.342 29
3.8	−739.368 87	−739.345 51	−739.320 22	−739.344 39
3.5	−739.381 31	−739.349 16	−739.312 97	−739.347 92
3.0	−739.408 66	−739.353 14	−739.294 63	−739.351 22
2.5	−739.438 00	−739.338 91	−739.263 14	−739.333 10
2.25	−739.444 74	−739.308 34	−739.264 08	−739.297 49
2.0	−739.430 08	−739.256 28	−739.240 63	−739.271 85

the diabatic potential is

$$^3A_2 \rightarrow V_d(r,\theta) = E^{\infty} + (1 - w(r))V_{lr}(r,\theta) + w(r)V_c(r) \quad (3)$$

The chemical potential has the form of Hase's stiff Morse function, and *w(r)* plays the role of a switching function

$$Vc(r) = D_e(1 - (1 - e^{-(\beta_0 + \sum \beta_i (r-r_e)^i)(r-r_e)})^2)w(r)$$

$$w(r) = 1/(1 + e^{-\gamma/(r-r_e)^2} e^{b(r-r_c)}) \quad (4)$$

The parameters β_i, γ, b, r_c, r_e, and D_e are determined by fitting to the ab initio potential, but $V_{lr}(r,\theta)$ is determined using the expressions given above and the experimental (μ,α) or computed (Q,$\alpha_\perp - \alpha_{||}$) parameters. It is essential that the accuracy of the long-range potential does not deteriorate. (r_e = 2.197 Å, b = 0.849 Å^{-1}, β_0 = 1.5201 D^{-1}, $\beta_1 = -1.213 \times 10^{-3}$ Å^{-2}, r_c = 4.98 Å^{-1}, γ = 2.885 Å^2, D_e = 211.2 kJ/mol.)

Note that for C_{2v} geometries, there is no difference between the diabatic and adiabatic potentials in the $^3B_1$ and $^3A_2$ states.

The second ingredient of our modeling is the coupling functions. We have proposed the following expressions:

$$H_{12}(r,\theta,\psi) = V_{12}(r)\cos^2(\psi)\sin^4(\theta)$$

$$H_{13}(r,\theta,\psi) = V_{13}(r)(1 + (\cos^2\psi - 1)\sin^2\theta)$$

$$H_{23}(r,\theta,\psi) = V_{23}(r)\cos^2(\psi)\sin^4(\theta)$$

$$H_{24}(r,\theta,\psi) = V_{24}(r)\sin^2(\psi)\sin^2(\theta)$$

$$H_{14} = H_{34} = 0$$

$$H_{ij} = H_{ji} \quad (5)$$

where the indices 1, 2, 3, and 4 refer to the states $^3B_2(0)$, $^3A_2$, $^3B_2(1)$, and $^3B_1$, respectively, and ψ is the angle assigned to the rotation of the SH_2 group about its symmetry axis, defined in such a way that it is 0 or π for nonplanar C_s geometries. These expressions have been chosen so that they have the correct behvior for symmetrical geometries and provide an adequate fitting to the ab initio data in the procedure to be described. The use of coupling functions was considered advantageous over interpolating on a set of numerical values; the expressions given above are by no means the only options and should not be viewed as a recipe for other similar cases. Coupling of the $^3B_1$ and both $^3B_2$ states is neglected altogether; this assumption is partly justified by the lack of a vibrational normal mode of A_2 symmetry in a four-atom system of C_{2v} symmetry, and it simplified the trajectory computations considerably.

The numerical values of the radial coupling functions $V_{ij}(r)$ are determined as follows: (i) trial values are given, and the matrix which collects diabatic potentials and coupling terms as nondiagonal elements is diagonalized; (ii) the resulting energy differences are compared to the ab initio energy differences, and the process is repeated until sufficient accuracy is reached

$$\begin{pmatrix} V_1 & H_{12} & H_{13} & H_{14} \\ H_{21} & V_2 & H_{23} & H_{24} \\ H_{31} & H_{32} & V_3 & H_{34} \\ H_{41} & H_{42} & H_{43} & V_4 \end{pmatrix} \rightarrow \{\Delta E_{ij}\}$$

$$\delta(|\Delta E_{ij} - \Delta E_{ij}^{\text{ab-initio}}|^2) \rightarrow \min \quad (6)$$

Of course, the symmetry is used to reduce the number of nonzero coupling terms. For instance, the values for V_{13} and V_{24} were determined in independent step. To obtain V_{24} the ab initio computations for planar C_s symmetries were made.

The following exponential functions resulted from the fitting to the numerical values (V_{ij} is in Hartrees and r in Å):

$$V_{12}(r) = -1.1959e^{-2.32025(r-3)} + 0.04436e^{-2.2246(r-4.5)}$$

$$V_{23}(r) = -0.48746e^{-1.8499(r-3)} + 0.03360e^{-1.7881(r-4.5)}$$

$$V_{13}(r) = 0.01691e^{-2.1257(r-3)} + 0.00100e^{-0.23335(r-4.5)}$$

$$V_{24}(r) = -0.00216e^{-0.8374(r-3)} + 0.000035e^{-3.5855(r-4.5)} \quad (7)$$

Finally, having obtained diabatic potentials and coupling functions, we can compute the PES; this is done by diagonalizing the matrix (eq 6). These are the PES employed in the dynamical computations of the capture step; this way, the value of the couplings, the diabatic potentials, and the PES themselves are fully consistent.

V. Approximate Classical Trajectory Computations

As stated above, the first step in the study of the reaction dynamics is a classical trajectory computation for the capture process. We employed the following Hamiltonian for the long-range region:

$$H_{lr} = \frac{p_r^2}{2\mu} + V_{\min}(R) + \frac{|\vec{J} - \vec{j}|^2}{2\mu R^2} + \frac{p_\theta^2}{2I} + \frac{(p_\theta - p_\psi \cos\theta)^2}{2I\sin^2\theta} + \frac{p_\psi^2}{2I_3} + V_o(R,\theta,\psi) \quad (8)$$

where the vectors $\vec{J}$ and $\vec{j}$ represent the total collision and rotational angular momentum, respectively. $V_{\min}(R)$ represents the minimum of the long-range potential for a particular value of R, the distance between the centers of mass, and $V_o(R,\theta,\psi)$ represents the orientation potential. Recall that θ and ψ represent the angle of the dipole moment with respect to the line connecting the centers of mass and the rotation angle of SH_2 about the symmetry axis (see, for instance, ref 28). The total potential would be, of course, $V(R,\theta,\psi) = V_{\min}(R) + V_o(r,\theta,\psi)$. I is the average moment of inertia ($I = \sqrt{I_1 I_2}$), μ is the reduced mass of collision, and p_r is the momentum associated with the coordinate R, while the other momenta correspond to the rotations of SH_2 and have the following expressions:

$$p_\psi = I_3(\dot{\phi}\cos\theta + \dot{\psi})$$

$$p_\phi = (I\sin^2\theta + I_3\cos^2\theta)\dot{\phi} + I_3\dot{\psi}\cos\theta$$

$$p_\theta = I\dot{\theta} \quad (9)$$

As stated above, the long-range potential is independent of ψ, so the $p_\psi^2/2I_3$ was assigned to AhK^2, A being the rotational constant corresponding to the symmetry axis. In addition, in the long-range region, the projection of the rotational angular momentum on the line connecting the centers of masses is given by the quantum number M; consequently, the rotational part of the Hamiltonian reduces to

$$H_r = \frac{p_\theta^2}{2I} + \frac{(M - K\cos\theta)^2\hbar^2}{2I\sin^2\theta} + \frac{(K\hbar)^2}{2I_3} + V_o(R,\theta) \quad (10)$$

The second term can be viewed as a θ-dependent effective potential.

Each trajectory has a particular set of quantum numbers, {J,j,M,K}, as well as a particular energy E. Values of j and M

are sampled, whereas K is given a thermally averaged value K_T. Each trajectory is also given values of the relative speed g and the impact parameter b; the orbital angular momentum ($l = \mu g b$) and the total energy are then determined. All possible couplings of rotational and orbital angular momenta are considered through the particular value of $J = \{|l - j|, ..., l + j\}$; J is considered to be a real number in practice. We chose to consider both J and j as good quantum numbers; the corresponding term in the Hamiltonian is then written as

$$\frac{|\vec{J} - \vec{j}|^2}{2\mu R^2} = \frac{\hbar^2}{2\mu R^2}[J(J+1) - 2M^2 + j(j+1)] \quad (11)$$

Note that this choice is consistent with the centrifugal sudden approximation.[25]

An initial value of θ is also necessary; we chose a random number limited by the roots of the following equation:

$$\dot{s}^2 = (1 - s^2)\left[(E_r - V_o(R_0,\theta))\frac{2}{I}\right] - \left(\frac{\hbar}{I}\right)^2 (M - sK)^2 \qquad s = \cos\theta \quad (12)$$

where R_0 is the initial value of the distance between the centers of mass and E_r is the rotational energy excluding AhK^2. The end of the long-range region depends on the trajectory and is reached when the former equation has less than two real roots with an absolute value of <1. This situation is a locked dipole. At this point, we switch to a two-dimensional rotor model, the corresponding Hamiltonian given basically as an expression similar to eq 10 but in which p_ϕ is not determined by the quantum number M. To keep the computation within a reasonable processing time, we have taken the energy corresponding to rotation about the symmetry axis as a constant. The centrifugal potential is now simply

$$\frac{|\vec{J} - \vec{j}|^2}{2\mu R^2} = \frac{\hbar^2}{2\mu R^2} J(J+1) \quad (13)$$

and the radial speed is adjusted to maintain a constant energy.

Nonadiabatic Transitions. Nonadiabatic transitions are treated through the so-called "anteater" model proposed by Tully and Preston.[26] When a trajectory reaches a seam, the probability of nonadiabatic crossing P is computed and compared to a random number ξ, $0 \le \xi \le 1$; if $P > \xi$,. the system "jumps" to the other surface in the seam. This procedure is repeated every time a seam is reached. The transition probability is computed through the Landau−Zener (LZ) and Rosen−Zener−Demkov (RZD) models[27]

$$P_{ij}^{LZ} = e^{-2\pi H_{ij}(R,\theta,\psi)^2/\hbar v_\perp(|\partial V_d(R,\theta)/\partial\xi_\perp)_1 - (\partial V_d(R,\theta)/\partial\xi_\perp)_2|)}$$

$$P_{ij}^{RZD} = \frac{1}{1 + e^{\pi\Delta_{ij}/\hbar\beta v_\perp}} \quad (14)$$

where $v_\perp$ is the velocity perpendicular to the seam,[28] $\xi_\perp$ and $\xi_{||}$ are coordinates perpendicular and parallel to the seam, respectively, $(\partial V_d(R,\theta)/\partial\xi_\perp)_1$ and $(\partial V_d(R,\theta)/\partial\xi_\perp)_2$ are the slopes of the diabatic potentials at both sides of the LZ seam, and H_{ij} is the coupling between diabatic potential surfaces. The Landau−Zener model can be applied to avoided crossings for low energies; in this case, we can better employ the adiabatic electronic states for the dynamics. It was originally developed for a one-dimensional two-state case. Lorquet and co-workers have extensively worked on its extension to multidimensional cases,[29] while Nakamura has carefully studied its applicability.[30,31] The LZ seam is located at the (R,θ) curve where the diabatic potentials cross; the diabatic potentials are independent of ψ. The ψ-dependent terms in the coupling functions are averaged to $^1/_2$ to compute the transition probability. The coordinates $\xi_\perp$ and $\xi_{||}$ are defined as follows:

$$\xi_\perp = R - f\theta \qquad \xi_{||} = \theta + R/f \quad (15)$$

where $f = (dR/d\theta)_s$, this derivative being the rate of variation of R with θ at the seam.

When an avoided crossing does not exist, the Rosen−Zener model, also called Demkov model, is employed. Originally, this model assumes that two adiabatic states asymptotically parallel start having a significant interaction and, consequently, diverge at a particular point in the reaction coordinate. Δ_{ij} is the long-range energy difference between potential surfaces, and β is the exponential parameter of the coupling term, which is assumed to have the form $V(R) = V_0 e^{-\beta R}$; we can replace β_2 with the exponential parameter of the second term in eq 7. The RZD seam is positioned at the (R,θ) line where the coupling function equals the absolute value of the difference between the diabatic potentials; in practice, the ψ-dependent factors in the coupling terms are averaged to $^1/_2$.

Both LZ and RZD types of crossings take place only between states of the same spatial symmetry; whether this condition is fulfilled or not depends on the molecular geometry. This requirement is partially taken into account by the angular dependence given to the coupling functions (eq 5).

The nonadiabatic transition implies a change in the potential, ΔV; to keep the total energy constant, we must change the speed. We basically follow Miller and George[32] and vary the speed of the movement perpendicular to the seam, i.e., $v_\perp = d\xi_\perp/dt$ while $d\xi_{||}/dt$ remains constant. This criterion is not met in some cases; it is not only the probability that determines whether a transition takes place. The change in speeds is given by the following equations:

$$\Delta\dot{R}^2(\mu + I/f^2)/2 + \Delta\dot{R}(\mu\dot{R} - I\dot{\theta}/f) + \Delta V = 0 \qquad \Delta\dot{\theta} = -\Delta\dot{R}/f \quad (16)$$

The transition will not take place unless the following condition is met:

$$\Delta V < \frac{(\mu\dot{R} + I\dot{\theta}/f)^2}{2(\mu + I/f^2)} \quad (17)$$

The velocity in the expressions of the transition probability is determined with the increments computed from former equations employing $\Delta V/2$ as variation of the potential.

VI. Results of the Trajectory Computations for the Capture Step

The lowest term of P^+ has three levels. The lowest level is $^3P_2$; $^3P_1$ and $^3P_0$ are 1.97 and 5.61 kJ/mol higher in energy, respectively.[33] These levels correlate with the C_{2v} states $^3A_2$, $^3B_2(1)$, and $^3B_1$, which are computed without taking into account spin−orbit interactions. Simple symmetry considerations indicate that each level correlates with the three C_{2v} states; these states may not become adequate representations until the energy difference between them, arising from the electric field exerted by the P^+ ion, is at least of a magnitude close to that of the spin−orbit splitting. It is assumed that the population of the C_{2v} states will be given by a thermal distribution at this point (d(P−S) = 6 Å). Also, the nonadiabatic transitions between the C_{2v} states are considered only for shorter P−S distances. This criterion excludes only the $^3A_2 - ^3B_2(1)$ transition because

TABLE 5: Capture Rate Coefficients (in 10^{-10} cm^3 s^{-1}) for the Three Electronic States of the Reactants at $T = 300$ K[a]

starting state	k_1	k_2	k_3	k_4	k_r	k_{et}
$^3B_1$	8.0	6.3	0.04	0.4	6.8	1.2
$^3B_2(1)$	6.4	0.2	0.4	0.03	3.2	3.2
$^3A_2$	10.8	1.2	0.08	1.3	9.4	1.4
total rate	9.3	1.3	0.17	0.9	7.4	1.9

[a] Indices 1−4 represent the $^3B_2(0)$,$^3A_2$,$^3B_2(1)$, and $^3B_1$ final states, respectively at long range. k_r and k_{et} correspond to the generation of $PSH_2^+(^3A'')$ and the electron-transfer products $P^+ + SH_2$.

the seam is located in the long-range region; the V_{23} function takes values much higher than those of V_{24}. We will make the approximation of neglecting the $^3B_2-^3B_1$ transitions.

The results for $T = 300$ K are displayed in Table 5. We must recall that the experimental rates for electron transfer and reaction (meaning production of PS^+ and $(PSH)^+$) are 0.4×10^{-9} and 1×10^{-9} cm^3 s^{-1}, respectively.[4,5] The three C_{2v} states corresponding to the reactants behave very differently.

The lowest-lying state corresponding to the reactants is of $^3A_2$ character at the long-range and, of course, the most populated according to our hypothesis (we will name states according to their symmetries for large P−S distances of C_{2v} geometries). It also appears to be the most reactive. The main reason for this is the conical intersection that connects the $^3A_2$ state to the ground state ($^3B_2(0)$ for large distances). Most of the trajectories starting in the $^3A_2$ state leak into the ground state through the conical intersection (CI); this mechanism accounts for most of the reactive flux

$$^3A_2 \rightarrow \mathbf{CI} \rightarrow PSH_2^+(^3A'')$$

The $^3A_2$ state also produces the electron-transfer products. The trajectories remaining on the $^3A_2$ state past the conical intersection rebound (R) at short range and go down to the ground state in the next passage through the intersection

$$^3A_2 \rightarrow \mathbf{CI} \rightarrow \mathbf{R} \rightarrow \mathbf{CI} \rightarrow {}^3B_2(0)$$

It is important to note that whenever the ground state is ,-derived, the transition to the upper states, including the second state, is sometimes not possible because the momentum transfer condition often may not hold. It is quite an important detail that the minimum for a particular value of R in the ground state appears at about $\theta \approx \pi/2$, whereas for the second state, it is located at $\theta \approx 0$. In the case of incoming trajectories, the SH_2 group is often rather well oriented, i.e., the dipole is "locked", with the rotation confined to maximum values of θ significantly lower than π, but after falling to the ground state, the average orientation is shifted to $\theta \approx \pi/2$. In this situation, not only is the transition probability low, the energy gap is positive and quite high in magnitude. In our modeling of the PES, this divergence with increasing angle is due mostly to the coupling junction. Finally, it should be noted that the capture rate of this state (1.36×10^{-9} cm^3 s^{-1}), computed by counting all trajectories reaching the short-range region (d(P−S) < 5 Å), is almost coincident with the experimental reaction rate, while $k_r + k_{et}$ is somewhat lower. This result is due in part to the fact that about 10% of the trajectories are deflected into the $^3B_1$ state and perhaps also due to inaccuracies in the computed PES, which might cause the capture flux to be too low. However, it is also possible that the models treating the nonadiabatic transitions are not accurate enough.

The third state of the manifold ($^3B_2(1)$ for large P−S distances) is much less reactive. This is due partly to the shape of the third PES, which folds quite rapidly with increasing θ. It delivers a lower flux to the region where the short-range nonadiabatic transitions take place. In addition, the probability of the 3−1 transition, which takes place at the locus of the avoided crossing, is generally somewhat low. The $^3B_2(0)$ state derived in this manner often undergoes transition into the second state ($^3A_2$) at the conical intersection, taking away some of the "reactive" flux, which is only partly recovered as electron-transfer flux. The mechanisms for electron transfer can be described as follows:

$$^3B_2(1) \rightarrow \mathbf{AC} \rightarrow \mathbf{R} \rightarrow \mathbf{AC} \rightarrow {}^3B_2(0)$$

$$^3B_2(1) \rightarrow \mathbf{AC} \rightarrow {}^3B_2(0) \rightarrow \mathbf{CI} \rightarrow {}^3A_2 \rightarrow \mathbf{R} \rightarrow \mathbf{CI} \rightarrow {}^3B_2(0) \rightarrow \mathbf{AC} \rightarrow {}^3B_2(0)$$

the first being more important.

The reaction flux is due to the following path:

$$^3B_2(1) \rightarrow \mathbf{AC} \rightarrow {}^3B_2(0) \rightarrow \mathbf{CI} \rightarrow PSH_2^+(^3A'')$$

According to our model, the reactivity of the $^3B_1$ state depends entirely on the effectiveness of the transition into the $^3A_2$ state, which occurs in the capture process before the conical intersection is reached. The $^3A_2$ state derived in this manner then undergoes the same processes described earlier. Recall also that the $^3A_2-^3B_1$ interaction is responsible for the depletion of the reactive or electron-transfer fluxes from the $^3A_2$ state.

It is clear that the total rate coefficient for the electron-transfer channel corresponding to the capture step k_{et} is lower than that of the experimental value, while our computed k_r is relatively close. As we will show, redissociation of the $PSH_2^+(^3A'')$ complex might bring the k_{et}/k_r ratio somewhat closer to the experimental value, but it is still quite deficient. A number of reasons might explain this deficiency. First, our computed PES might not be accurate enough, particularly to provide an adequate energy difference between both $^3B_2$ states, which is essential for an adequate modeling of the avoided crossing. Note that the $^3B_2(1)$ state delivers the highest electron-transfer flux, whereas it has by far the lowest capture flux. Of course, we could try to improve the ab initio computations by upgrading the basis sets and using better reference wave functions, but we believe that this would not be sufficient. The inclusion of the spin−orbit and other interactions is of essential importance. It would also be important to ascertain whether these kind of improvements would cause a short-range RZD seam for the $^3A_2-^3B_2(1)$ interaction. Also, the treatment of the ψ angle may be improved. Our experience suggests that averaging ψ-dependent terms to $^1/_2$ in the expressions of the coupling functions is probably quite correct, for the PES do not vary too much with R in the region where transitions take place. However the fact that $^3B_2-^3B_1$ transitions are not allowed is likely to cause a significant reduction of the flux into the $^3B_2(1)$ state; this effect probably contributes to keeping the k_{et}/k_r ratio too small. Finally, the models employed (RZD and LZ) are, admittedly, quite limited. We would stress, however, that approximate treatments based on them, like the one pursued in this work, are valuable to identifying the main processes and providing a reasonably adequate starting point for the study of the rearrangement and fragmentation processes of the collision complex.

VII. RRKM Computations of the Evolution of the $(PSH_2)^+$ Complex

The trajectory computations produce the distribution function *f(E,J)* for the population of levels of total energy and angular

momentum; those corresponding to reactive collisions were selected for our RRKM-type computations instead of the thermal distribution. The implicit assumption of this treatment is that the ergodic hypothesis can be applied (meaning, in this context, that there is unrestricted energy flow between degrees of freedom). Although it would be preferable to continue the trajectory computations on the potential surfaces of the $(PSH_2)^+$ complex, such a treatment is extremely difficult to apply given the complexity of the PES, not only in this case but in almost any ion−molecule reaction of this kind. However, it could be precisely this complexity and the occurrence of nonadiabatic transitions through conical intersections that will often make statistical treatments applicable.[29] In general, the applicability of RRKM-type computations for high-energy ions is, in most cases, well established. In our case, the formation of the high-energy complex is not instantaneous (meaning in the femtosecond time scale) but occurs in a collision, and the transition states are so low with respect to the typical energies of the complex that the energy can be considered as a quasicontinuum. However, it will be ultimately necessary to check the results by comparing them with experimental results and trajectory computations on reliable PES. The present case is very interesting because we have two different products, $PS^+(^1\Sigma) + H_2$ and $(PSH)^+(^2A') + H$, for which we have experimental branching ratios at $T = 300$ K. Details of the type of approach employed are given in earlier work[34] (actual values of vibrational frequencies, rotational constants, position of variational transition states, etc., are available upon request). It should be noted that although individual rate coefficients might not be very accurate (their values may depend significantly on the details of the computation), their ratio should be much more reliable.

We have considered the following processes for the dissociation of the $PSH_2^+(^3A'')$ complex:

(1) $PSH_2^+(^3A'') \rightarrow P + SH_2^+(^2B_1)/P^+ + SH_2(^1A_1)$

(2) $PSH_2^+(^3A'') \rightarrow TST1/P(H)SH^+(^3A) \rightarrow HPSH^+(^3A)$

(3) $PSH_2^+(^3A'') \rightarrow TST2/PSH{-}H^+(^3A) \rightarrow PSH^+(^2A') + H$

(4) $PSH_2^+(^3A'') \rightarrow TST3/PS^+{-}H_2(^3A'') \rightarrow PS^+(^3\Sigma) + H_2$

Isomerization into the $HPSH^+$ form may also entail intersystem crossing and produce $HPSH^+(^1A')$ instead of $HPSH^+(^3A)$. The latter intermediate may evolve through the following processes:

(5) $HPSH^+(^3A) \rightarrow TST4/HPS^+{-}H(^3A') \rightarrow HPS^+(^2A') + H$

(6) $HPSH^+(^3A) \rightarrow TST5/H{-}PSH^+(^3A) \rightarrow PSH^+(^2A') + H$

(7) $HPSH^+(^3A) \rightarrow TST6/HP(H)S^+(^3A) \rightarrow H_2PS^+(^3A'')$

(8) $HPSH^+(^3A) \rightarrow TST7/P(H_2)S^+(^3A') \rightarrow PS^+(^3\Sigma) + H_2$

(9) $HPSH^+(^3A) \rightarrow TST1/P(H)SH^+(^3A) \rightarrow PSH_2^+(^3A'')$

Finally, $SPH_2^+(^3A'')$ may undergo the following reactions:

(10) $SPH_2^+(^3A'') \rightarrow HPS^+(^2A') + H$

(11) $SPH_2^+(^3A'') \rightarrow TST8/SP^+{-}H_2(^3A) \rightarrow PS^+(^3\Sigma) + H_2$

(12) $SPH_2^+(^3A'') \rightarrow TST6/HP(H)S^+(^3A) \rightarrow HPSH^+(^3A)$

As mentioned, we have assumed that intersystem crossing may take place in the third process after transition-state TST1 passes, so we also studied the evolution of $HPSH^+(^1A')$. It was found in a similar case (reaction of P^+ with water[9]) that the PO^+/POH^+ branching ratio could be explained if singlet $HPOH^+$ was assumed to be the intermediate which generated both products. We will show that this is also the case in the present reaction. Note that the formation of $PS^+(^3\Sigma) + H_2$ is only slightly exothermic.

TABLE 6: Rate Coefficients (in ps^{-1}) for the Evolution of the Reaction Intermediates Computed at $T = 300$ K

$PSH_2^+(^3A'')$		$HPSH^+(^3A)$		$H_{2PS}^+(^3A'')$		$HPSH^+(^1A')t$		$H_2PS^+(^1A_1)$	
k_1	0.20	k_5	24	k_{10}	9.7	k_{13}	0.66	k_{17}	0.033
k_2	1.25	k_6	12	k_{11}	0.29	k_{14}	0.58	k_{18}	0.016
k_3	0.45	k_7	2.8	k_{12}	1.9	k_{15}	3.7	k_{19}	4.5
k_4	0.008	k_8	0.004			k_{16}	0.052		
		k_9	4.0						

Singlet $HPSH^+(^1A')$ may be subjected to the following processes:

(13) $HPSH^+(^1A') \rightarrow TSS2/HP(H)S^+(^1A) \rightarrow SPH_2^+(^1A_1)$

(14) $HPSH^+(^1A') \rightarrow TSS3/P(H_2)S^+(^1A') \rightarrow PS^+(^1\Sigma) + H_2$

(15) $HPSH^+(^1A') \rightarrow HPS^+(^2A') + H$

(16) $HPSH^+(^1A') \rightarrow PSH^+(^2A') + H$

One of the processes involves isomerization into $SPH_2^+(^1A_1)$. This species may isomerize back into $HPSH^+(^1A')$ or generate both products

(17) $SPH_2^+(^1A_1) \rightarrow HPS^+(^2A') + H$

(18) $SPH_2^+(^1A_1) \rightarrow TSS4/SP^+{-}H_2(^1A') \rightarrow PS^+(^1\Sigma) + H_2$

(19) $SPH_2^+(^1A_1) \rightarrow TSS2/HP(H)S^+(^1A) \rightarrow HSPH^+(^1A')$

We have not found saddle points for processes 1, 10, 15,16, and 17; the transition states were determined variationally by minimizing the canonical rate coefficients along the reaction coordinates. In the last four processes, the reaction coordinates have been determined by locating the minima corresponding to a series of values of the S−H or P−H bond distances at the UMP2=full/6-31G(d) level. Using these sets of geometries, we have computed the energy profiles at the spin-projected UMP2 level[35] with a 6-311+G(3df,2p) basis set, (PMP2/6-311+G(3df,2p), the PMP2 wave functions have rather small spin contamination). The transition between vibration and rotation along these reaction coordinates was treated with a sinusoidally hindered model which also includes steric interactions, as formulated by Gilbert and co-workers.[36]

Table 6 shows that the rate of process 1 is not negligible compared to those of processes 2−4; according to these values, about 10% percent of the trajectories would result in either $P + SH_2^+(^2B_1)$ or $P^+ + SH_2(^1A_1)$. This result partly explains why the experimental branching ratio corresponding to the electron-transfer process is not that consistent with the outcome of the study of the capture process. The generation of any of the other products from $PSH_2^+(^3A'')$ is only significant in the case of $PSH^+(^2A')$ (23%), but the main process is rearrangement through TST1, which, if our hypothesis is correct, will ultimately lead to $HPSH^+(^1A')$. Note that the existence of some degree of nonergodicity should normally result in a greater accumulation of energy in the P−S bond, which would increase the electron-transfer rate at the cost of reducing the reaction rate (the rate of

generation of $(PSH)^+$ and PS^+) and the total rate because the reactants would also be regenerated in the bond-breaking process.

The main points about the evolution of $HPSH^+(^3A)$ are that (i) the generation of $PS^+(^3\Sigma)$ is very slow and (ii) the generation of HPS^+ and, especially, PSH^+ are extremely fast processes (in fact, the speed of the latter cannot be computed accurately by RRKM theory). Isomerization into the other triplet species is also fast, but its speed does not even approximate that of the latter processes. $HPSH^+(^3A)$, whenever it is formed, may produce only HPS^+/PSH^+ without even evolving into the other triplet species, so the generation of PS^+ should entail the participation of another intermediate. We also computed the rates of fragmentation for $SPH_2^+(^3A'')$, but these are largely irrelevant, for this region of the triplet PES would hardly be reached. In conclusion, if intersystem crossing were not an important process in the isomerization of $PSH_2^+(^3A'')$ (all trajectories would remain in the triplet PES), the $PS^+/(PSH)^+$ branching ratio could not be explained.

For the study of the evolution of $HPSH^+(^1A')$, we have given the rates corresponding to the trans isomer; those corresponding to the cis form are quite similar. The formation of the products $PS^+(^1\Sigma) + H_2$ and $PSH^+(^2A')$ is much faster than the other processes, including isomerization into $SPH_2^+(^1A_1)$. Note the rather small rate of formation of $HPS^+(^2A')$. This is due mainly to steric hindrances in the reaction path caused by the closure of the <HPS bond angle with increasing S−H distance. The latter effect may be due to contamination by the electron configurations that are dominant in the TSS2 structure. We have detected, however, that the degree of hindrance is quite sensitive to the level of computation, so we would consider the PSH^+/HPS^+ ratio to be quite uncertain. Note, however, that the saddle point connecting the latter two species is 7.9 kcal/mol higher in energy than $PSH^+(^2A')$ at the G2(QCI) level. This result implies that isomerization would not possible in interstellar space conditions (which normally preclude reactions with an activation barrier),[37] for the latter species would not have enough energy.

The rearrangement of $HPSH^+(^1A')$ back into a singlet or triplet PSH_2^+, as computed using the TSS2 structure, has a rate coefficient $k = 0.4\ ps^{-1}$, clearly lower than that of process 15.

The most important point is that the $PSH^+(^2A')/PS^+(^1\Sigma)$ branching ratio computed approximately as $(k_{15} + k_{16})/k_{14}$ is not very high, about 6.5, not even too far from the experimental value (4.8).[5] Although more sophisticated computations would be necessary to obtain an accurate branching ratio, even within the RRKM framework, it is quite clear that both products can be generated from $HPSH^+(^1A')$ in proportions roughly consistent with the experimental value. $PSH^+(^2A')$ does not have to be generated mainly through a triplet intermediate, the branching ratio then reflecting the efficiency of an instersystem crossing process. According to our rate coefficients, the lower the efficiency of the intersystem crossing process, the higher the branching ratio is. Consequently, our results clearly suggest that intersystem crossing takes place early in the rearrangement of $PSH_2^+(^3A'')$ and is probably a very efficient process so that the reaction may take place almost exclusively along the singlet PES from that point.

VIII. Conclusions

The reaction of P^+ with hydrogen sulfide has been studied through an approximate classical trajectory method to deal with the capture process and a RRKM-type approach for the evolution of the $(PSH_2)^+$ complex. Nonadiabatic transitions have been taken into account in the capture step through the Landau−Zener and Rosen−Zener−Demkov models. Potential surfaces were computed through the G2(QCI) method in the case of local minima and saddle points, whereas the MR-AQCC and PMP2 methods were applied to determine the energy profiles. Reaction energies were computed with the CBS-Q and CBS-QB3 models in addition to G2(QCI).

Two mechanisms were found to be responsible for the generation of the electron-transfer products—namely, the rebound on repulsive potential surfaces in the capture step accompanied by transition to the lowest-lying surface and the breaking of the P−S bond of the $PSH_2^+(^3A'')$ intermediate, the former being more important. The experimental PSH^+/PS^+ branching ratio cannot be explained without the lowest-lying singlet PES playing a major role. In fact, our results suggest that both products could be the result of the fragmentation of $HPSH^+(^1A')$, which appears to be the global minimum. This kind of conclusion was also encountered in a previous study of the $P^+ + H_2O$ reaction.

We expect that more work will be done on other similar reactions to shed light on some of the uncertainties about the dynamics of ion−molecule reactions. Some of them are (i) the role of repulsive potential surfaces in the capture step, (ii) the role of bond breaking of reaction intermediates in the generation of electron-transfer products, and (iii) the role of intersystem crossing processes in the evolution of the complex.

Acknowledgment. The authors acknowledge financial support from the government of the autonomous community of Galicia (project PGIDT99PXI30102B) and the Spanish Ministry of Education (project PB98-1085).

References and Notes

(1) Smith, D.; Spanel, P. *Mass Spectrom. Rev.* **1995**, *14*, 255.
(2) Ng, C.-Y., Baer, M., Eds. In *State-Selected and State to State Ion-Molecule Reaction Dynamics*, Parts 1 and 2; In *Advances in Quantum Chemistry*; Prigogine, I., Rice, S. A., Series Eds.; John Wiley, New York, 1992; Vol. 82.
(3) Phillips, L. F. *Prog. Energy Combust. Sci*. **1992**, *18*, 75.
(4) Smith, D.; McIntosh, B. J.; Adams, N. G. *J. Chem. Phys*. **1989**, *90*, 6213.
(5) Adams, N. G.; McIntosh, B. J.; Smith, D. *Astron. Astrophys*. **1990**, *232*, 443.
(6) Dateo, C. E.; Clary, D. C. *J. Chem. Phys*. **1989**, *90*, 7216.
(7) Clary, D. C.; Dateo, C. E.; Smith, D. *Chem. Phys. Lett*. **1990**, *167*, 1.
(8) Chase, M. W., Jr. NIST-JANAF Thermochemical Tables, 4th ed.; *J. Phys. Chem. Ref. Data*. **1998**, 1−1951; Monograph 9. (http://webbook.nist.gov)
(9) Flores, J. R.; Redondo P. *Chem. Phys. Lett.* **1994**, *230*, 358.
(10) Jensen, F. *Introduction to Computational Chemistry*; John Wiley: New York, 1999.
(11) Curtiss, L. A.; Carpenter, J. E.; Raghavachari, K.; Pople, J. A *J. Chem. Phys.* **1987**, *87*, 5968.
(12) Curtiss, L. A.; Raghavachari, K.; Trucks, G. W.; Pople, J. A. *J. Chem. Phys*. **1991**, *94*, 7221.
(13) Durant, J. L., Jr.; McMichael Rohlfing, C. *J. Chem. Phys*. **1991**, *98*, 8031
(14) Roos, B. O. In *Ab Initio Methods in Quantum Chemistry*; Lawley, K. P., Ed.; John Wiley: New York, 1987; Vol. 2.
(15) Woon, D. E.; Dunning, T. H., Jr. *J. Chem. Phys*. **1993**, *98*, 1358.
(16) Szalay, P. G.; Bartlett, R. J. *Chem. Phys. Lett.* **1993**, *214*, 481.
(17) Gdanitz, R. L.; Ahlrichs, R. *Chem. Phys. Lett.* **1988**, *143*, 413.
(18) Shepard, R.; Shavitt, I.; Pitzer, R. M.; Comeau, D. C.; Pepper, M.; Lischka, H.; Szalay, P.; Ahlrichs, R.; Brown, F. B.; Zhao, J. G. *Int. J. Quantum Chem: Quantum. Chem. Symp*. **1988**, *22*, 149.
(19) Frisch, M. J.; Trucks, G. W.; Schlegel, H. B.; Gill, P. M. W.; Johnson, B. G.; Robb, M. A.; Cheeseman, J. R.; Keith, T.; Petersson, G. A.; Montgomery, J. A.; Raghavachari, K.; Al-Laham, M. A.; Zakrzewski, V. G.; Ortiz, J. V.; Foresman, J. B.; Cioslowski, J.; Stefanov, B. B.;

Nanayakkara, A.; Challacombe, M.; Peng, C. Y.; Ayala, P. Y.; Chen, W.; Wong, M. W.; Andres, J. L.; Replogle, E. S.; Gomperts, R.; Martin, R. L.; Fox, D. J.; Binkley, J. S.; Defrees, D. J.; Baker, J.; Stewart, J. P.; Head-Gordon, M.; Gonzalez, C.; Pople, J. A. *Gaussian94*; Gaussian: Pittsburgh, PA, 1995.

(20) López, X.; Ugalde, J. M.; Barrientos, C.; Largo A.; Redondo. P. *J. Phys. Chem.* **1993**, *97*, 1521−1525.

(21) Ochterski, J. W.; Petersson, G. A.; Montgomery, J. A., Jr. *J. Chem. Phys*. **1996**, *104*, 2598.

(22) Montgomery, J. A., Jr.; Frisch, M. J.; Ochterski, J. W.; Petersson, G. A. *J. Chem. Phys*. **1999**, *110*, 2822.

(23) Buckingham, A. D. In *Intermolecular Forces*; Hirschfelder, J. O., Ed.; John Wiley: New York, 1967.

(24) Bates, D. R.; Morgan, W. L. *J. Chem. Phys*. **1987**, *87*, 2611.

(25) Pack, R. T. *J. Chem. Phys*. **1974**, *60*, 633.

(26) Tully, J. C.; Preston, R. K. *J. Chem. Phys.* **1971**, *55*, 562.

(27) Nakamura, H. In *Dynamics of Molecules and Chemical Reactions*; Wyatt, R. E., Zhang, J. Z. H., Eds.; Marcell Dekker: New York, 1996.

(28) Desouter-Lecomte, M.; Dehareng, D.; Leyh-Nihant, B.; Praet, M. Th.; Lorquet, A. J.; Lorquet, J. C. *J. Phys. Chem.* **1985**, *89*, 214.

(29) Lorquet, J. C. In *The Structure, Energetics and Dynamics of Organic Ions*; Baer, T., Ng, C.-Y, Powis, I., Eds.; John Wiley: New York, 1996.

(30) Nakamura, H. In *State-Selected and State-to-State Ion-Molecules Reaction Dynamics*, Part 2; Ng, C.-Y., Baer, M., Eds; In *Advances in Quantum Chemistry*; Prigogine, I., Rice, S. A., Series Eds.; John Wiley: New York, 1992; Vol. 82.

(31) Nakamura, H. *J. Chem. Phys.* **1987**, *87*, 4031.

(32) Miller, W. H.; George, T. F. *J. Chem. Phys*. **1972**, *56*, 5637.

(33) *CRC Handbook of Chemistry and Physics*; Lide, D. R., Ed.; CRC Press: Boca Raton, FL, 1998.

(34) Flores, J. R.; Redondo, P. *Mol. Phys*. **1997**, *92*, 743.

(35) Schlegel, H. B. *J. Phys. Chem*. **1988**, *92*, 3075.

(36) Gilbert, R. G.; Smith, S. C. *Theory of Unimolecular and Recombination Reactions*; Blackwell Scientific Publications: Oxford, 1990.

(37) Duley, W. W.; Williams, D. A. *Interstellar Chemistry*; Academic Press: New York, 1984.